NJC

ROYAL SOCIETY OF CHEMISTRY

PERSPECTIVE

Cite this: *New J. Chem.*, 2021, **45**, 19622

Chalcogenides as photocatalysts

Ashmalina Rahman and Mohammad Mansoob Khan *

Chalcogenides are narrow-band gap semiconductors that have been widely used as photocatalysts. These narrow-band gap materials allow more efficient absorption of over 40% of solar energy in the visible light range, which will eventually improve its photocatalytic properties. Under visible light irradiation, these materials generate electron and hole (e^-/h^+) pairs. Photo-generated e^-/h^+ pairs have been utilized to split water into hydrogen and oxygen and to remove and degrade industrial, pharmaceutical and agricultural organic/inorganic/biological pollutants that have been accumulated in the environment. In this perspective review, different types of chalcogenides, namely, binary, multinary (ternary and quaternary) and chalcogenide-based heterostructures are presented briefly. This perspective review also highlights the mechanisms involved and remarkable photocatalytic activity enhancement under visible light irradiation that has been widely researched such as the photocatalytic degradation of industrial pollutants and photocatalytic inactivation of bacteria. Lastly, future prospects for the use of chalcogenides as photocatalysts and chalcogenide-based heterostructures were discussed.

Received 10th September 2021,
Accepted 30th September 2021

DOI: 10.1039/d1nj04346c

rsc.li/njc

Introduction

Semiconductors are materials whose conductivity lies between those of conductors (such as metals) and non-conductors/insulators (such as ceramics). Metal oxides and chalcogenides are two of the widely researched semiconductor materials. TiO_2 and ZnO metal oxides are mainly used as photocatalysts due to their non-toxicity, low cost, stability and resistance to photo-corrosion.[1] Despite their stability, the major drawback of using metal oxides as photocatalysts is their wide band gap energy. The wide band gap energy enables them to absorb only ultra-violet light (around 4% of the solar energy), which limits their wide practical applications.[2,3] Many approaches have been were employed to develop materials with a narrow band gap energy.[4]

Chalcogenides are well known for their narrow band gap energy. Chalcogenides are compounds consisting of at least one chalcogen anion (S^{2-}, Se^{2-} or Te^{2-}) and at least one electro-positive element.[5] Chalcogenides have drawn significant attention due to their great and highly demanded properties including narrow band gap energy, non-toxicity, bio-compatibility, low cost and facile synthesis.[6,7] Researchers have developed different synthesis routes including solvothermal,[8] hydrothermal,[9] hot injection,[10] and sol–gel[11] methods for the preparation of chalcogenides. The utilization of novel semiconductors such as chalcogenides and chalcogenide-based materials has been widely reported because of their narrow band gap energy which enables them to utilize light in the visible region.[12]

Photocatalysis is the most effective and cleanest way in coping with environmental and energy issues. Hence, developing suitable photocatalysts that could respond to visible light is highly necessary. Fig. 1 shows the examples of photocatalytic activities.

This mini review will assist the readers to obtain and overview the classification of chalcogenides (namely, binary, multinary and chalcogenide heterostructures) and the recent progress in the application of chalcogenides as visible light-driven photocatalysts.

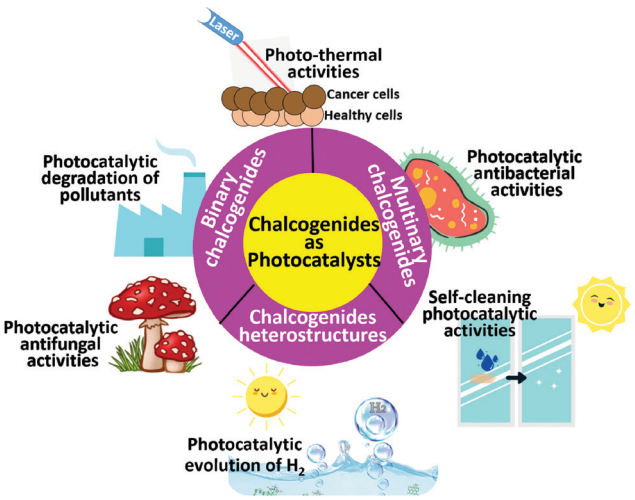

Fig. 1 Examples of different photocatalytic activities using chalcogenides.

Chemical Sciences, Faculty of Science, Universiti Brunei Darussalam, Jalan Tungku Link, Gadong, BE 1410, Brunei Darussalam. E-mail: mmansoobkhan@yahoo.com, mansoob.khan@ubd.edu.bn

In addition, a review of the complex processes/mechanisms involved, in particular, in some complicated ternary or quaternary photocatalysts is also proposed, and this will undoubtedly promote the further development and research in this area. Finally, the future prospects and conclusion are also highlighted.

Chalcogenide-based photocatalysts are narrow-band gap semiconductors, which upon irradiation with light, generated e^-/h^+ and reactive oxygen species that could degrade organic/inorganic pollutants or biological pollutants such as microorganisms (listed in Table 1).

There are several factors to be considered in the fabrication of chalcogenide-based photocatalysts in order to achieve appreciable photocatalytic efficiency, which are as follows:

(1) Light harvesting capability of the synthesized materials: the materials should be designed to absorb light in the visible light region by tuning the band gap energy.

(2) High separation efficiency of the photo-generated charge carriers.

(3) Better migration of these photo-generated charge carriers to the surface, where the reaction occurs.

(4) Controlled growth and assembly of the materials with high surface area-to-volume ratio: this will increase the reactive sites of the synthesized materials and, therefore, improve the photocatalytic activities.

(5) Stable under prolonged exposure to light: the stability of the materials should be high in order to prevent the materials from photo-corrosion.

Photocatalytic mechanisms of different types of chalcogenides

Binary metal-based chalcogenides

Chalcogenide compounds falling into this category consist of only one chalcogen and one electropositive atom. Based on the literature review, binary chalcogenides have been successfully prepared and used for photocatalysis. For instance, Ain *et al.* have successfully synthesized hexagonal CuS nanoplates using copper(II) dithiocarbamate as a precursor and octylamine as a decomposing solvent.[13] The synthesized CuS nanoplates exhibited a band gap energy of 2.1 eV and showed enhancement up to 100% degradation of Congo red under irradiation of light within 40 min. In another study, Cu_2Se with a band gap energy of 2.25 eV was able to degrade up to 98.2% of methylene blue within 1 h under irradiation of visible light. Khan *et al.* have prepared Ag_2Se sonochemically, capped it with starch and functionalized it with folic acid.[51] The synthesized materials showed high affinity towards A549 tumor cells (it targeted the tumor cells selectively), and the materials successfully reduced the tumor volume in mice within 30 days. Moreover, the utilization of hydrothermally synthesized In_2S_3 for visible light-driven photocatalytic inactivation of *E. coli* has been reported by Qiu *et al.*[52] In_2S_3 with a narrow band gap of 2.25 eV have shown remarkable inactivation efficiency toward *E. coli* under fluorescent tube irradiation. Furthermore, the mechanism involved in binary metal-based chalcogenides is shown in Fig. 2. When photons with enough energy ($h\nu \geq E_g$) hit a photocatalyst, the photo-generated e^-/h^+ pairs will promptly appear. The photo-generated e^- will be promoted to the conduction band (CB) leaving behind h^+ in the valence band (VB). From the reaction of the e^- in the CB and adsorbed O_2 molecules on the surface of the photocatalyst, superoxide ($O_2^{-\bullet}$) will be generated. Simultaneously, the reactive hydroxyl radicals ($OH^\bullet$) will also be produced *via* the reaction with h^+ in the VB.[53]

The conduction band of binary metal-based chalcogenides is mainly affected by the orbitals of the metal (for example, if the metal used is a transition metal, then the conduction band is mainly caused by the d-orbitals of the transition metal), whereas the valence band will be mainly affected by the p-orbitals of chalcogens (sulfide, selenide and telluride).

However, the studies of binary chalcogenides have been declining in popularity in recent years, mainly due to the difficulties in simultaneously obtaining favorable energy band alignments and recombination of charge carriers. Nonetheless, common strategies for enhancing the performance of binary photocatalysts under visible light irradiation are worth mentioning, which involve the manipulation of native defects, the optimization of surface area, morphology and crystal structure or the introduction of dopants in order to tune their optical and electronic properties. For instance, Yanalak *et al.* have successfully synthesized Ni, Co, Zn and Mn-doped Ag_2S nanocrystals *via* a hot-injection route. The band gap energies of Ag_2S, Zn-doped Ag_2S, Mn-doped Ag_2S, Ni-doped Ag_2S and Co-doped Ag_2S were found to be 2.23, 2.20, 2.13, 2.12 and 2.12 eV. After 8 h of irradiation under visible light, the average amount of hydrogen produced increases in the order of Ag_2S < Mn-doped Ag_2S < Zn-doped Ag_2S < Ni-doped Ag_2S < Co-doped Ag_2S with the highest hydrogen production of 5314 μmol g^{-1}.[54]

Multinary metal–based chalcogenides (ternary and quaternary chalcogenides)

The research on ternary and quaternary chalcogenides is an efficient strategy to overcome the intrinsic limitations of binary chalcogenides. It is suitable to improve the separation of photo-generated e^-/h^+ pairs, hindering their recombination. Multinary chalcogenides exhibited higher photocatalytic performance than that of binary chalcogenides because of the presence of three (ternary) or four (quaternary) elements, which enable them to delay the recombination of photo-generated e^-/h^+ pairs. For instance, Li and co-workers have prepared $Zn_{0.5}Cd_{0.5}S$ by a thermolysis method and reported that the synthesized ternary chalcogenides exhibited the highest H_2 evolution rate of 7.42 mmol h^{-1} g^{-1}, exceeding that of pristine CdS and ZnS by more than 24 and 54 times, respectively, and even much higher than that of optimal Pt-loaded CdS (4.70 mmol h^{-1} g^{-1}).[55]

Multinary metal-based chalcogenides could be further divided into ternary and quaternary chalcogenides. Ternary chalcogenides may be a combination of: (1) one electropositive atom and two chalcogens either S^{2-} or Se^{2-} or Te^{2-} and (2) two electropositive atoms and one chalcogen either S^{2-} or Se^{2-} or Te^{2-}. However, quaternary chalcogenides may be a combination of (1) one electropositive atom and three chalcogens

Table 1 Use of chalcogenides as photocatalysts

No.	Classification of chalcogenides	Chalcogenides used	Band gap energy (eV)	Photocatalytic activities	Source of light	Results	Ref.
1	Binary	CuS	2.1 eV	Photocatalytic degradation of Congo red	Solar light	Complete degradation within 80 min	13
2	Binary	Sb_2S_3	Indirect = 1.54 eV Direct = 1.72 eV	Photocatalytic degradation of methyl orange	UV lamp (4 W) visible light (under direct sunlight)	Dark = 7.4% UV light = 22% Visible light = 47%	14
3	Ternary	(Mo–Bi)S_x supported on mesoporous CdS	Not mentioned	Photocatalytic reduction of CO_2 to HCOOH	Xe lamp equipped with an optical filter (λ = 420–780 nm)	Formation rate of HCOOH reached 208 μmol g^{-1} h^{-1} with a 72% faradaic efficiency	15
4	Ternary	$AgBiSe_2$	Not mentioned	Photoelectric conversion efficiency	Under simulated sunlight with an intensity of 100 mW cm^{-2}	$AgBiSe_2$ exhibited a reduced resistance of 0.53 Ω m and markedly 50% improved absorption efficiency under monochromatic light	16
5	Ternary	Ba_2ZnSe_3	2.75 eV	Photocatalytic degradation of rhodamine B	Xe-lamp	Ba_2ZnSe_3 exhibited photocatalytic degradation about 20% rhodamine B within 240 min	17
6	Ternary	$BaAu_2S_2$	2.49 eV	Photocatalytic degradation of rhodamine B	1000 W Xe lamp coupled with 420 filters (λ > 420 nm)	45% of rhodamine B degraded after 240 min	18
7	Ternary	Bi-doped $CuGaS_2$	$CuGaS_2$ = 2.3 eV Bi-doped $CuGaS_2$ = 1.7 eV	Photoelectrocatalytic reduction of nitrobenzene	100 mW cm^{-2} Xe lamp	83% of nitrobenzene were photoelectrochemically converted into aniline	19
8	Ternary	Citrate-modified $CuFeS_2$	Not mentioned	Photocatalytic degradation of bisphenol A	4 W six fluorescent lamps	Exhibited high photocatalytic degradation of bisphenol A up to 97.4% within 60 min	20
9	Ternary	Cu_2SnS_3 and Cu_2SnSe_3 quantum dots were grown *in situ* on reduced graphene oxide (rGO)	Cu_2SnS_3 = 1.52 eV Cu_2SnSe_3 = 1.31 eV	Photocatalytic degradation of rhodamine B and methyl orange	300 W Xe lamp equipped with a 400 nm cutoff filter was used as the visible light source	Photocatalytic degradation of rhodamine B: TiO_2 P25 (Degussa) = 23.1% Cu_2SnS_3 = 65.1% Cu_2SnSe_3 = 49.3% Cu_2SnS_3/rGO = 96.3% Cu_2SnSe_3/rGO = 88.7% Photocatalytic degradation of methyl orange: TiO_2 P25 (Degussa) = 10.3% Cu_2SnS_3 = 57.3% Cu_2SnSe_3 = 45.1% Cu_2SnS_3/rGO = 94.3% Cu_2SnSe_3/rGO = 84.5%	21
10	Ternary	Cu_2SnSe_3–Au	—	Photocatalytic degradation of methylene blue	Xe lamp equipped with cut-off filter 400 nm	Cu_2SnSe_3–Au exhibited up to 80% photocatalytic degradation of methylene blue after 90 min under visible light	22
11	Ternary	Cu_2WS_4	2.15 eV	Photocatalytic removal of Cr(VI)	250 W Xe lamp and λ > 420 nm cut-off filters	Exhibited high removal of Cr(VI) up to 99% after 150 min	23
12	Ternary	$CuFeS_2$	Not mentioned	Photocatalytic degradation of tartrazine dye	85 W fluorescent lamp	Decolorization efficiency: 99.1% after 40 min Mineralization efficiency: 87.3% after 150 min	24
13	Ternary	Fe-doped $ZnIn_2S_4$	$ZnIn_2S_4$ = 2.12 eV Fe-$ZnIn_2S_4$ = 2.05 eV	Photocatalytic degradation of 2,4,6-tribromophenol	UV light (20 W Hg lamp with the light intensity of 297 W cm^{-2}) Visible light (100 W, tungsten-halogen and the light intensity was 1925 mW cm^{-2})	Pseudo-first-order constants were in the order of TiO_2 (0.022 min^{-1}) < 0.5 wt% $FeTiO_2$ (0.0369 min^{-1}) < $ZnIn_2S_4$ (0.362 min^{-1}) < 0.5 wt% Fe–$ZnIn_2S_4$ (0.436 min^{-1})	25
14	Ternary	Ru-loaded Cu_2WS_4	Cu_2WS_4 = 2.1 eV	Photocatalytic hydrogen production	300 W Xe lamp combined with a 430 nm cutoff filter	The highest activity for H_2 evolution reached up to 135 μmol h^{-1}	26

Table 1 (*continued*)

No.	Classification of chalcogenides	Chalcogenides used	Band gap energy (eV)	Photocatalytic activities	Source of light	Results	Ref.
15	Quaternary	Cu_2FeSnS_4	At different substrate temperature 160 °C = 1.62 eV 200 °C = 1.05 eV 240 °C = 1.46 eV 280 °C = 1.58 eV	Photocatalytic degradation of methylene blue	Under sun and Xe light	Cu_2FeSnS_4 thin film grown at temperature of 240 °C exhibited the highest photocatalytic degradation rate of methylene blue under sun light = 81%	27
16	Quaternary	$Cu_2ZnSnSe_4$	~1.4 eV	Photocatalytic degradation of rhodamine B	300 W Xe lamp equipped with a 420 nm cutoff filter	~90% rhodamine B degraded within 120 min	28
17	Heterostructure	$Ag/Ag_2S/CuS$	Not mentioned	Photocatalytic degradation of 2,4-dichlorophenol	300 W Xe lamp with a 420 nm cutoff filter	Exhibited up to 82% degradation after 240 min	29
18	Heterostructure	$Ag_2S/AgInS_2$	$AgInS_2$ = 1.73 eV Ag_2S = 1.10 eV $Ag_2S/AgInS_2$ core–shell heteronanoflowers (In/Ag =1 : 1, molar ratio) = 1.46 eV	Photocatalytic degradation of methyl orange	Visible light	Ag_2S = 8% $AgInS_2$ = 45% $Ag_2S/AgInS_2$ = 80%	30
19	Heterostructure	$AgInS_2$ quantum dots/In_2S_3	Not mentioned	Photon-to-current conversion efficiency	Illumination of simulated sunlight (100 mW cm^{-2}) provided by a solar simulator	Maximum photon-to-current conversion efficiency of about 37%	31
20	Heterostructure	$AgInS_2/SnIn_4S_8$	$AgInS_2$ = 1.69 eV $SnIn_4S_8$ = 1.75 eV (0.2 : 1) $AgInS_2$/$SnIn_4S_8$ = 1.86 eV (0.4 : 1) $AgInS_2$/$SnIn_4S_8$ = 1.79 eV (0.6 : 1) $AgInS_2$/$SnIn_4S_8$ = 1.65 eV (0.8 : 1) $AgInS_2$/$SnIn_4S_8$ = 1.77 eV (1 : 1) $AgInS_2$/$SnIn_4S_8$ = 1.81 eV	Photocatalytic degradation of 2-nitrophenol and tetracycline hydrochloride	Visible light	65.98% mineralization efficiency	32
21	Heterostructure	$AgInS_2/TiO_2$ composites	$AgInS_2$ = 1.75 eV TiO_2 = 3.30 eV $AgInS_2/TiO_2$ = 2.75 eV	Photocatalytic degradation of gaseous *o*-dichlorobenzene	500 W Xe lamp equipped with a UV-cut off filter ($\lambda > 400$ nm)	$AgInS_2/TiO_2$ exhibited the highest photocatalytic degradation up to 50.4% after 8 h	33
22	Heterostructure	$AgInS_2$–TiO_2	TiO_2 = 3.18 eV 0.5% $AgInS_2$–TiO_2 = 3.14 eV 1% $AgInS_2$–TiO_2 = 3.04 eV 2% $AgInS_2$–TiO_2 = 2.94 eV 5% $AgInS_2$–TiO_2 = 2.58 eV	Photocatalytic degradation of doxycycline	125 W high-pressure mercury vapor lamp	95% of doxycycline degradation was achieved within 180 min	34
23	Heterostructure	$CdS/Au/TiO_2$	Not mentioned	Photocatalytic degradation of norfloxacin	35 W Xe lamp	After 60 min of visible light irradiation $CdS/Au/TiO_2$ = 64.67% CdS/TiO_2 = 55.94% Au/TiO_2 = 50.60% TiO_2 = 42.04% norfloxacin degraded	35

Table 1 (*continued*)

No.	Classification of chalcogenides	Chalcogenides used	Band gap energy (eV)	Photocatalytic activities	Source of light	Results	Ref.
24	Heterostructure	CdS@MoS_2 core@shell	CdS = 2.18 eV MoS_2 = 1.61 eV	Photocatalytic degradation of rhodamine B	300 W Xe lamp was used as a light source with a 420 nm light filter to obtain visible light 5($\lambda \geq$ 420 nm)	79.60%	36
25	Heterostructure	CdSe/rGO heterojunction	CdSe = 2.3 eV CdSe@5% rGO = 1.95 eV CdSe@10% rGO = 1.81 eV CdSe@15% rGO = 1.78 eV CdSe@20% rGO = 1.77 eV	Photocatalytic oxidative desulfurization of thiophene	Visible light was illuminated by a 125 W medium pressure Hg lamp with an optical filter blocks the light of wavelengths <420 nm	CdSe = 40% CdSe@5% rGO = 50% CdSe@10% rGO = 79% CdSe@15% rGO = 100%	37
26	Heterostructure	CdX (X = S, Se and Te) quantum dots/TiO_2	TiO_2 = 3.11 eV CdS–TiO_2 = 2.20 eV CdSe–TiO_2 = 2.48 eV CdTe–TiO_2 = 2.81 eV	Photocatalytic degradation of benzene	300 W Xe-arc lamp as a source of visible-light irradiation	CdS–TiO_2 = 95% CdSe–TiO_2 = 90% CdTe–TiO_2 = 86%	38
27	Heterostructure	Co_3O_4/CoTe	Co_3O_4 = 1.5–2.5 eV CoTe = 2.24 eV	Photocatalytic degradation of Congo red	300 W Xe arc lamp having a UV cut-off filter was used as light source	Co_3O_4 and CoTe (1 : 1) composite = 96%	39
28	Heterostructure	$CuCaAg_2Se$/graphene/TiO_2	$CuCaAg_2Se$ = 2.76 eV Graphene/TiO_2 = 2.97 eV $CuCaAg_2Se$/graphene/TiO_2 = 2.79 eV	Photocatalytic reduction of CO_2 to methanol	500 W metal halide lamp	Yielded 12.68 and 16.84% of methanol under irradiation of visible and UV light, respectively after 48 h	40
29	Heterostructure	$CuCo_2S_4$/RGO nanocomposites	1.5 eV	Photocatalytic degradation of malachite green	500 W tungsten halogen lamp	3% of RGO loaded on $CuCo_2S_4$ exhibited the highest degradation up to 92% of the dye in 360 min	41
30	Heterostructure	CuS, Ag_2S and MoS_2 loaded on $ZnIn_2S_4$	$ZnIn_2S_4$ = 2.64 eV	Photocatalytic water splitting and photocatalytic degradation of methyl orange	300 W Xe arc lamp equipped with a cut-off filter ($\lambda >$ 400 nm)	Photocatalytic water splitting: CuS loaded $ZnIn_2S_4$: 14.95, μmol h^{-1} Ag_2S loaded $ZnIn_2S_4$: 15.86 μmol h^{-1} MoS_2 loaded $ZnIn_2S_4$: 47.71 μmol h^{-1} Photocatalytic degradation of methyl orange: MoS_2 loaded $ZnIn_2S_4$ exhibited up to 84% degradation of methyl orange	42
31	Heterostructure	CuS/NiO	CuS = 1.58 eV NiO = 3.2 eV	Photocatalytic production of H_2 in the presence of different organic substances dispersed in water (alcohols, amine and organic acids)	Natural sunlight	CuS@30% of NiO = 52.3 mmol h^{-1} g^{-1} H_2 gas from lactic acid-based electrolyte	43
32	Heterostructure	CuS@rGO	1.97 eV	Photocatalytic degradation of atrazine, toxic herbicide	300 W Xe lamp with $\lambda <$ 410 nm cut-off sieve	Complete degradation after 20 min	44
33	Heterostructure	MoS_2/Cu–$ZnIn_2S_4$	—	Photocatalytic H_2 production	300 W Xe lamp quipped with an UV cut-off filter ($\lambda >$ 420 nm)	5463 μmol h^{-1} g^{-1} H_2 evolution rate under visible light irradiation	45

Table 1 (*continued*)

No.	Classification of chalcogenides	Chalcogenides used	Band gap energy (eV)	Photocatalytic activities	Source of light	Results	Ref.
34	Heterostructure	SnS_2/SnO_2	SnO_2 = 3.59 eV Synthesized using 6 mmol thioacetamide, SnS_2/SnO_2-A = 2.27 eV 7.5 mmol thioacetamide, SnS_2/SnO_2-B = 2.22 eV 9 mmol thioacetamide, SnS_2/SnO_2-C = 2.21 eV SnS_2 = 2.19 eV	Photocatalytic removal of Cr(VI)	250 W Xe lamp and $\lambda > 420$ nm cut-off filters	SnS_2/SnO_2-B exhibited the highest photocatalytic activity of nearly 99% after 40 min	46
35	Heterostructure	TiO_2 wrapped (shell) onto CdSe (core) nanocapsule	—	Photocatalytic generation of H_2	Xe arc lamp with UV cut off filter $\lambda > 420$ nm used for UV and visible light irradiation	TiO_2 shell wrapped on CdSe NC performed a four-fold high quantity of H_2 gas (21 mmol h^{-1} g^{-1}) generation compared to pristine CdSe (5 mmol h^{-1} g^{-1}) with 12.9% visible light to H_2 fuel conversion efficiency under 328 mW cm^{-2} light intensity of visible light irradiation	47
36	Heterostructure	TiO_2/Cu–In–S/ZnS quantum dots-polysaccharide nanohybrids	Not mentioned	Photoelectrochemical solar cell	LED light with an intensity of 3 mW cm^{-2}	The photocurrent density produced is nearly 0.85 μA cm^{-2}	48
37	Heterostructure	$ZnIn_2S_4/MoO_3$ heterojunction	MoO_3 = 2.92 eV $ZnIn_2S_4$ = 2.24 eV	The photocatalytic degradation of methyl orange, rhodamine B and paracetamol	500 W halogen lamp	$ZnIn_2S_4/MoO_3$ composite exhibited 98% degradation within 80 min	49
38	Heterostructure	ZnO@Ag_2S core/shell	Ag_2S = 1.10 eV ZnO = 3.20 eV	Photocatalytic antimicrobial activities against selected *B. subtilis* (ATCC 6633), *E. coli* (ATCC 25922) and *C. albicans* (ATCC 10231)	Xe lamp (50 W) which was equipped with a UV cut-off filter to provide light emission at 400–800 nm	ZnO@Ag_2S exhibited the best efficiency against *E. coli* (Gram negative bacteria) with the lowest MIC value of 25 μg mL^{-1} as compared to efficiencies against *B. subtilis* (Gram-positive bacteria) and *C. albicans* (fungi)	50

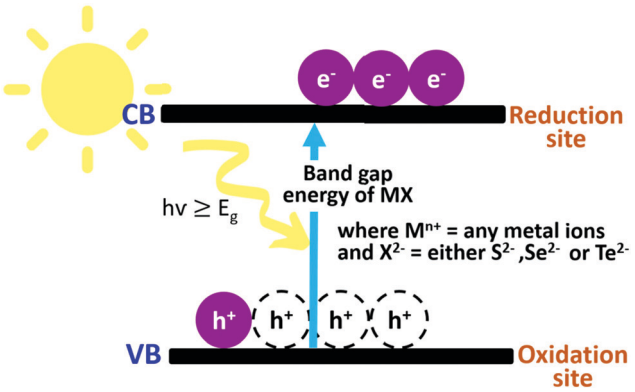

Fig. 2 Mechanism of photocatalysis for binary chalcogenides.

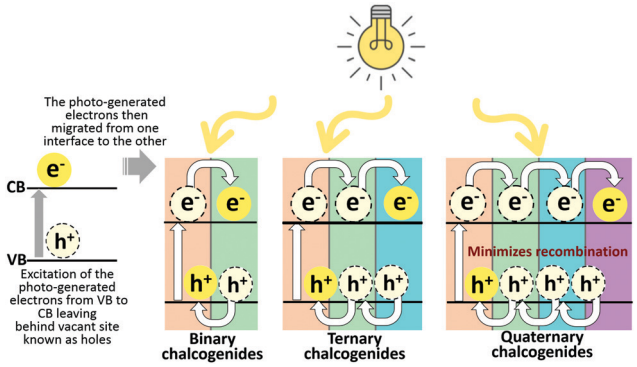

Fig. 3 Illustration of interfacial separation and transfer of charge carriers (e^- and h^+) in binary, ternary and quaternary chalcogenides.

either S^{2-} or Se^{2-} or Te^{2-}, (2) two electropositive atoms and two chalcogens either S^{2-} or Se^{2-} or Te^{2-} and (3) three electropositive atoms and one chalcogen either S^{2-} or Se^{2-} or Te^{2-}.

In another study, Yuan *et al.* have reported that solvothermal-assisted synthesis of MoS_2/Cu–$ZnIn_2S_4$ showed enhanced transfer and separation of charge carriers based on the largely increased photocurrent responses. MoS_2/Cu–$ZnIn_2S_4$ showed the highest photocatalytic activity with a H_2 production rate 72 times higher than that of bare Cu–$ZnIn_2S_4$ under visible light irradiation.[45] Another approach to generate more photoelectrons, improve the separation of e^-/h^+ pairs, and enhance the absorption of light into the visible region is by coupling the chalcogenide with a noble metal. Wang *et al.* reported that Cu_2SnSe_3–Au synthesized by a seed-mediated growth method showed a higher rate of photocatalytic degradation of methylene blue than that of pure Cu_2SnSe_3.[22] After 90 min of irradiation under visible light, Cu_2SnSe_3–Au was able to degrade 80% of methylene blue, whereas pure Cu_2SnSe_3 degraded only 50%. They reported that it may be due to the synergetic effects of the Schottky junction and appropriate band alignment of the Cu_2SnSe_3–Au composite, which promote efficient transfer and separation of the charge carriers. An example of quaternary chalcogenide is Cu_2FeSnS_4. Nefzi and co-workers have successfully synthesized Cu_2FeSnS_4 by spray pyrolysis technique on glass substrates at different substrate temperatures (T_s = 160, 200, 240 and 280 °C). They reported that a Cu_2FeSnS_4 thin film grown at 240 °C showed the highest photocatalytic degradation rate of methylene blue (81%) under sunlight irradiation for 4 h.[27] Fig. 3 shows the interfacial separation of charge carriers in different types of chalcogenides when used as photocatalysts.

Furthermore, in multinary chalcogenides, the orbitals that are responsible for the conduction and valence bands are different in comparison to the binary metal-based chalcogenide. For example, the valence band of quaternary Cu_2ZnSnS_4 consists of hybridized sulfide-p and copper-d orbitals, while the conduction band is derived from the hybridization of sulfide-s/p and Sn-s orbitals.[56]

Doping of chalcogenides

Doping is one of the strategies used to overcome the instability problem upon light illumination, and photo-corrosion or photo-dissolution that may occur during photocatalytic reactions. Both metals and non-metals can be used as dopants to modify chalcogenides to overcome its drawbacks.[57–60] Zhu and co-authors have synthesized carbon nitride-derived carbon and nitrogen co-doped CdS which has effectively promoted the stability of the material hindering the photo-corrosion of CdS under illumination of visible light.[61] In some cases, doping is also used to improve the ability of chalcogenides to harvest visible light. For instance, ZnS is a wide band gap chalcogenide (~3.6 eV) that requires UV light for its excitation. Gaikwa *et al.* have reported that the doping of ZnS with Pd results in increased photocatalytic activity of ZnS due to the improved visible light absorption and increased surface area of the synthesized materials.[62] The authors also reported that the doping of ZnS with Pd caused the generation of energy levels/defect levels within the band gap of ZnS. The introduction of Pd in the ZnS modified its band structure by strong hybridization between Pd 4d and S 3p valence states, which results in the widening of the valence band and narrows the band gap energy, as shown in Fig. 4.

Metal ion dopants can also induce defects that can enhance charge separation and transfer, thereby improving the photocatalytic performance. Moreover, the additional trap states could prevent spontaneous recombination of the charge carriers,

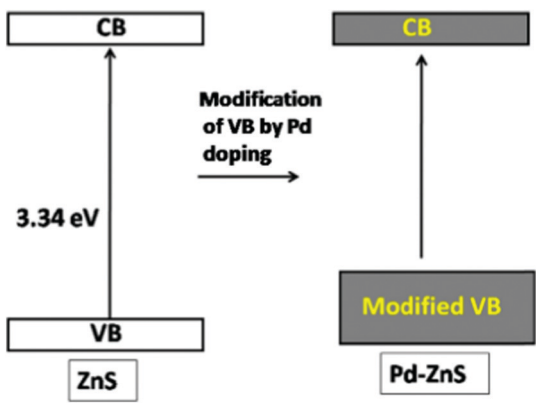

Fig. 4 Illustration of the modification of ZnS band gap energy when doped with Pd.[62]

thus extending the lifetime of electrons and holes. Metal co-doping in CdS with nickel and cerium, for example, shows enhanced photocatalytic degradation of rhodamine B up to 90% within 2 h upon exposure to visible light.[63] The enhancement may be due to generation of new trapping defect sites as a result of the incorporation Ni/Ce dopants, which lead to a reduction in the rate of e^-/h^+ pair recombination. In another study, Yang and co-workers have doped CdS with Zn by a hydrothermal method.[64] The 0.1 Zn/Cd molar ratio exhibited the highest photocatalytic degradation of methylene blue up to 92.8% within 240 min. They reported that the incorporation of metal ions, in this case Zn^{2+} may generate a Schottky barrier, which acts as charge carrier trap. This prolongs the life span of the charge carriers and ensures better utilization of the charge carriers, thus improving the photocatalytic performance. However, high doping percentages could create recombination centers that may decrease the number of active charge carriers. The same research group reported that when the molar ratio of Zn/Cd was higher than the optimal value, Zn doping became detrimental. It may be because of the increase in the recombination rate due to the decrease in the distance between trapping sites in a particle.[64] It has also been observed that co-doping with different elements is often more effective than single or mono-doping for improving the photocatalytic performance.

Chalcogenide-based heterostructures

(a) Coupling of chalcogenides with metal oxides. The formation of composites with a heterojunction interface between the semiconductors with matching band potentials is another approach to promote the separation of photo-generated charge carriers and enhance their lifetime, improving the photocatalytic efficiency. The presence of multicomponent heterojunctions could possibly aid in the delaying/preventing recombination of these photo-generated charge carriers by effectively enhancing the interfacial charge transfer.[65]

Owing to the multiple separation of photo-generated carriers (due to the presence of multiple heterojunctions), the chalcogenide-based heterostructures exhibited greater photocatalytic activity in comparison to the binary and multinary chalcogenides. The examples of chalcogenide-based heterostructures are the coupling of chalcogenides with carbon-based materials (such as graphenes and carbon nanotubes) or the surface modification of chalcogenides with MXenes or with another semiconductor, *i.e.* metal oxides or with noble metals. For instance, a $CuCaAg_2Se$–graphene–TiO_2 nanocomposite has been successfully synthesized by Otgonbayar *et al.* using a hydrothermal method.[40] These materials showed 6 times higher photocatalytic CO_2 reduction to methanol in comparison to TiO_2, graphene–TiO_2 and pure $CuCaAg_2Se$ nanomaterials under irradiation of UV and visible light. Moreover, $CuCaAg_2Se$–graphene–TiO_2 displayed excellent stability with no obvious loss in the production of methanol from a CO_2 recycling photoreduction test.

In some cases, during irradiation, both photocatalysts can be excited with photo-generated charge carriers depending on the band gap energy. Usually under visible light irradiation, the e^- produced in narrow-band gap semiconductors with less positive CB can be transferred quickly to the more positive CB of the photocatalyst with the wider band gap semiconductor. However, the photo-excited h^+ from wide-band gap semiconductor could be shifted easily into the valence band (VB) of the narrow-band gap semiconductor. As reported by Zhao *et al.*, the photocatalytic reduction of Cr(VI) up to 98.7% has been successfully carried out using a MoS_2/ZnS/ZnO composite within 90 min.[66] The excellent photocatalytic activity is attributed to the presence of dual-type heterojunctions, which hinder the recombination of e^-/h^+ pairs, resulting in fast electron transfer and high efficiency of e^-/h^+ separation. As proposed, upon irradiation of light, the photo-generated e^- of MoS_2 and ZnS move to the CB of ZnO due to the difference in electronic potentials (the CB position of ZnO is more positive/less negative than that of MoS_2 and ZnS), which also enables the h^+ on the VB of ZnO to be injected to the VB of MoS_2 and ZnS, respectively. The chalcogenide-based heterostructures have shown a slightly different photocatalytic mechanism, and the mechanism involved is shown in Fig. 5.

(b) Coupling of chalcogenides with metals. The deposition of metals onto the surface of chalcogenides could promote efficient separation and transfer of photo-generated carriers to the reaction sites, which could greatly reduce the chances of recombination. The functions of deposited metals are to provide a path to speed up the transfer of charge carriers. Moreover, its surface could act as a charge trap center/sink to host more active sites for photo-reaction. Fig. 6 shows the photocatalytic mechanism of metal@chalcogenide heterostructures.

For instance, Mao *et al.* have successfully prepared Pt–Ru bimetals synthesized *via* a two-step chemical reduction route on CdS for the photocatalytic evolution of H_2.[67] They reported that the H_2 evolution rate of Pt–Ru/CdS is 18.35 mmol h^{-1} $g_{cat.}{}^{-1}$, which is 1.7 and 2.9 times higher than those of Pt/CdS and Ru/CdS, respectively. These noble metals played an important role in trapping the photo-generated e^-, which promotes the separation efficiency of the photo-generated carriers. In another study, Zheng and co-workers have prepared Ni/(Au@CdS) core–shell photocatalysts *via* selective transformation of benzyl alcohol to benzaldehyde and H_2 under visible light.[68] The synthesized materials exhibited excellent transformation activity under light

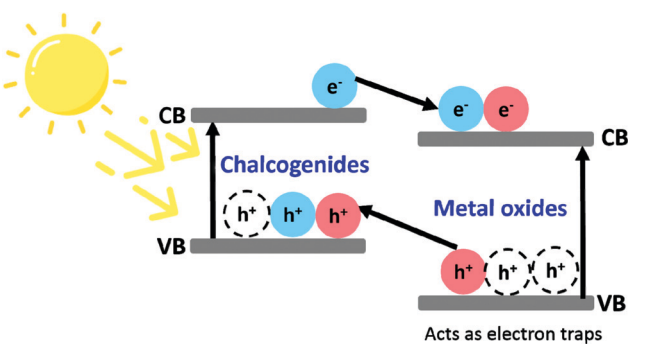

Fig. 5 Mechanism of photocatalysis of chalcogenide-based heterostructures by coupling with metal oxides.

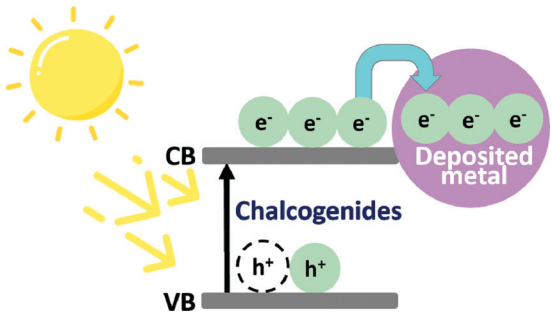

Fig. 6 Mechanism of photocatalysis of metal@chalcogenide heterostructures.

and yielded H_2 and benzaldehyde with yields up to 3882 and 4242 μmol g^{-1} h^{-1}, respectively. The enhanced activity is due to the enhanced utilization efficiency of visible light and accelerated separation of photo-generated e^-/h^+ pairs, as a result of plasmon-induced resonance energy of Au cores as well as the ability of loaded Ni on CdS shells that could capture the e^- and serve as the effective active sites for proton reduction and H_2 evolution.

(c) Coupling of chalcogenides with carbon-based materials. One of the key strategies to overcome rapid photo-generated charge carrier recombination is the coupling of the narrow-band gap chalcogenides with carbon-based materials. Examples of the various carbon-based materials used in improving the photocatalytic activities of chalcogenides are shown below:

(i) Graphene and graphene oxide. Graphene has carbon hexagons consisting of sp^2 hybridized C–C bonding with π-electron clouds. Graphene exhibits large specific surface area, chemical stability, excellent mechanical property and high charge carrier mobility, making it a perfect base material. rGO is another important variant of graphene, consisting of few-atom-thick 2D sp^2 hybridized carbon layers with fewer oxygeneous functionalities. It has been reported that rGO could help improve carrier separation, charge transport, and stability in a photocatalytic system. The general photocatalytic mechanism of chalcogenides coupled with graphene-based materials is shown in Fig. 7.

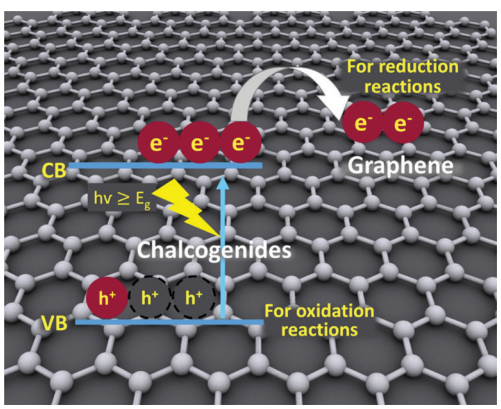

Fig. 7 Mechanism of photocatalysis of the chalcogenide coupled with rGO.

Alhaddad *et al.* have successfully utilized CuS@rGO heterojunctions to completely degrade atrazine herbicide after 20 min under visible light irradiation.[44] The authors reported that the photo-generated e^- from CuS was transferred to rGO, where it acted as a sink and thus enhanced the separation of the charge carriers. In addition, the formation of reactive oxygen species ($^{\bullet}O_2^-$ and $^{\bullet}OH$ radicals) can react with the adsorbed atrazine molecules on the photocatalyst active sites, generating harmless products; CO_2, NO_3^-, Cl^- and H_2O. Another example is reported by Salarizadeh and co-workers, they have synthesized MoS_2/NiS/Co_3S_4/$CoMo_2S_4$/reduced graphene oxide by a hydrothermal method.[69] This study demonstrated that the incorporation of reduced graphene oxide into MoS_2/NiS/Co_3S_4/$CoMo_2S_4$ enhances the electrochemical surface area for urea electrooxidation, which resulted in a higher current density (18 mA cm^{-2}) than pure MoS_2/NiS/Co_3S_4/$CoMo_2S_4$ (3.7 mA cm^{-2}). Moreover, Mkhalid *et al.* have showed the reduction of the band gap energy of CdSe from 2.3 eV to 1.78 eV when 15 wt% of rGO was coupled to CdSe.[37] They showed that 15 wt% rGO/CdSe material exhibited 100% photocatalytic oxidation of thiophene after 90 min of light exposure. The excellent performance may be due to the enhancement in visible light absorption and improvement of the separation of the photo-generated charge carriers.

(ii) Graphitic carbon nitride. Graphitic carbon nitride (g-C_3N_4) has gained much interest due to its thermal stability, chemical resistance, biocompatibility, and visible light photocatalytic and electro-catalytic properties. Balapure and co-workers have reported the excellent antimicrobial performance of Ag_2S/g-C_3N_4 nanocomposites against *E. coli* and *S. aureus* under visible light.[70] They reported that the synthesized nanocomposites exhibited up to 99.9% of antimicrobial property against *E. coli* after 40 min of light irradiation, and a similar trend in the bactericidal efficacy was also observed against *S. aureus* after 3 h. The high bactericidal activities under visible light irradiation were majorly attributed to the formation of reactive oxygen species ($^{\bullet}OH$ and $^{\bullet}O_2^-$ radicals). In another study, Zuo *et al.* reported that Ag_2S/g-C_3N_4 p–n heterojunctions synthesized *via* an *in situ* deposition approach exhibited notable photocatalytic activities in the inactivation of *E. coli* and *S. aureus* under visible light irradiation.[71] The pristine single Ag_2S and g-C_3N_4 showed a poor inactivation performance for *E. coli* (only 1.8 and 1.1 log of cells were inactivated, respectively), while the composite could completely deactivate 7.0 log of *E. coli* in 90 min. A similar trend was observed against *S. aureus.* The enhanced bacterial inactivation activities were also owing to the synergistic effect of the generated radicals.

(iii) MXenes. MXenes are 2D transition metal carbides or nitrides ($M_{n+1}X_nT_x$) derived from ternary transition metal carbide or nitride materials, the so-called MAX phase, ($M_{n+1}AX_n$), where M represents an early transition metal. MXenes have received much attention for their superior conductivity, better hydrophilicity and quite strong interfacial synergistic effects. For instance, Chen and co-workers have employed MXenes as media to transport e^-

between CdS and MoS_2 for the photocatalytic evolution of hydrogen.[72] The CdS/MoS_2/MXene exhibited a H_2 generation rate of 9679 μmol g^{-1} h^{-1} and showed enhancement up to 251.3% in comparison to CdS/MoS_2. This study showed the promotion ability of the synthesized materials and it may be ascribed to the increased transfer and separation of photo-generated e^-/h^+ pairs. In another study, Liang and co-authors have constructed 2D/1D Ti_3C_2/CdS nanorod composites for photocatalytic reduction of uranium(VI) with the highest removal of 97% with 5% Ti_3C_2 after 40 min.[73] They reported that Ti_3C_2 plays an important role in enhancing the photocatalytic activity as well as improving the photocorrosion resistance of CdS due to the strong interaction between MXenes and Cd^{2+}, which prevents Cd^{2+} from leaching.

These materials (carbon-based materials, MXenes, metals and other semiconductors) could act as electron traps, which provide sites for the accumulation of electrons and then improve the separation of e^-/h^+ pairs. The modification of chalcogenides *via* surface modification is the effective way to tune the band gap energy of chalcogenides, facilitate the separation of photo-generated charge carriers, reduce the recombination of these carriers and, thus, improve the photocatalytic activities.

To summarize, it is possible to fabricate chalcogenide-based photocatalysts that provide excellent light-harvesting performance and able to resist photo-corrosion. It is needed to develop eco-friendly new materials that are resistant to photo-corrosion and will not dissolve in water; specifically, toxic metals such as Cd and Pb, or these unstable chalcogenides will be impractical for real-life applications. Furthermore, there is still lack of detailed studies in relation to reusing/recycling chalcogenide-based photocatalysts. Moreover, the results from the photolysis of pollutants under light conditions should always be included in order to make a reasonably comparison with actual photocatalytic activities. Besides these, external factors could influence the photocatalytic performance of the materials, which include the photo-reactor used, light intensity, the distance between the set-up and the light, photocatalyst dosage, concentrations and types of model pollutants, and other experimental conditions.

Future outlook

Even though a steady progress in utilizing chalcogenides as photocatalysts has been achieved, there are still a range of challenges that need to be addressed in order to promote and gain interests from other researchers in this area of study:

• Although many works on the use of chalcogenides as photocatalysts have been reported, the photo-corrosion issue is yet to be explored. The exact cause of photo-corrosion of these materials should be thoroughly researched in order to synthesize high-quality, high-stability and multifunctional chalcogenides.

• Low-cost and large-scale synthesis methods of chalcogenides also required attention. The optimization of different parameters in the reaction synthesis such as different sources of precursors, temperature, pH, and reaction time should also be studied for optimal yield in order to facilitate the production of these materials at a commercial scale.

• An in-depth study to extend the life of photo-generated carriers and mitigate the recombination of these charged carries is still required in order to improve the photocatalytic efficiency of these materials for broader applications. Several approaches that could be employed include coupling with other semiconductors, loading of noble metals, and doping with metals.

Conclusion

Chalcogenides have been emerging as promising materials for visible light-induced photocatalysis. These materials have been synthesized and investigated thoroughly. Chalcogenides show excellent properties for many potential applications such as water splitting, hydrogen production, light harvesting, and photocatalytic bacterial inactivation. Chalcogenide-based photocatalysts have attracted the attention of researchers because of their narrow band gap energy, visible light harvesting ability and various applications including solar energy utilization, visible light-induced photocatalysis, visible light-assisted water splitting, optoelectronic devices and removal of hazardous pollutants. Additionally, recent studies have reported that the enhancement in the photocatalytic activities was caused by the surface modification of these materials. The modification of chalcogenides provides multiple heterojunctions to extend the life of photo-generated charge carriers and/or to provide electron traps to reduce the recombination of e^-/h^+ pairs.

Conflicts of interest

Authors declare that there is no conflict of interest.

Acknowledgements

Authors would like to acknowledge the FIC block grant UBD/RSCH/1.4/FICBF(b)/2021/035 received from Universiti Brunei Darussalam, Brunei Darussalam.

References

1 A. Rahman, M. H. Harunsani, A. L. Tan and M. M. Khan, Zinc Oxide and Zinc Oxide-Based Nanostructures: Biogenic and Phytogenic Synthesis, Properties and Applications, *Bioprocess Biosyst. Eng.*, 2021, 0123456789, DOI: 10.1007/s00449-021-02530-w.

2 S. Matussin, M. H. Harunsani, A. L. Tan and M. M. Khan, Plant-Extract-Mediated SnO_2 Nanoparticles: Synthesis and Applications. *ACS Sustain*, *Chem. Eng.*, 2020, **8**(8), 3040–3054, DOI: 10.1021/acssuschemeng.9b06398.

3 M. Hojamberdiev, Y. Cai, J. J. M. Vequizo, M. M. Khan, R. Vargas, K. Yubuta, A. Yamakata, K. Teshima and M. Hasegawa, Binary Flux-Promoted Formation of Trigonal $ZnIn_2S_4$ Layered Crystals Using ZnS-Containing Industrial

Waste and Their Photocatalytic Performance for H_2 Production, *Green Chem.*, 2018, **20**(16), 3845–3856, DOI: 10.1039/C8GC01746H.

4 M. M. Khan, S. F. Adil and A. Al-Mayouf, Metal Oxides as Photocatalysts, *J. Saudi Chem. Soc.*, 2015, **19**(5), 462–464, DOI: 10.1016/j.jscs.2015.04.003.

5 M. Bouroushian, *Chalcogens and Metal Chalcogenides*, 2010, pp. 1–56, DOI: 10.1007/978-3-642-03967-6_1.

6 Y. I. Choi, S. Lee, S. K. Kim, Y.-I. Kim, D. W. Cho, M. M. Khan and Y. Sohn, Fabrication of ZnO, ZnS, Ag-ZnS, and Au-ZnS Microspheres for Photocatalytic Activities, CO Oxidation and 2-Hydroxyterephthalic Acid Synthesis, *J. Alloys Compd.*, 2016, **675**, 46–56, DOI: 10.1016/j.jallcom.2016.03.070.

7 M. E. Khan, M. M. Khan and M. H. Cho, CdS-Graphene Nanocomposite for Efficient Visible-Light-Driven Photocatalytic and Photoelectrochemical Applications, *J. Colloid Interface Sci.*, 2016, **482**, 221–232, DOI: 10.1016/j.jcis.2016.07.070.

8 K. Saravanan, S. Selladurai, S. Ananthakumar, S. Moorthy Babu and R. Suriakarthick, Solvothermal Synthesis of Copper Cadmium Sulphide ($CuCdS_2$) Nanoparticles and Its Structural, Optical and Morphological Properties, *Mater. Sci. Semicond. Process.*, 2019, **93**(September 2018), 345–356, DOI: 10.1016/j.mssp.2019.01.024.

9 S. Kannan, P. Vinitha, K. Mohanraj and G. Sivakumar, Antibacterial Studies of Novel Cu_2WS_4 Ternary Chalcogenide Synthesized by Hydrothermal Process, *J. Solid State Chem.*, 2018, **258**, 376–382, DOI: 10.1016/j.jssc.2017.11.005.

10 A. Sarilmaz, M. Can and F. Ozel, Ternary Copper Tungsten Selenide Nanosheets Synthesized by a Facile Hot-Injection Method, *J. Alloys Compd.*, 2017, **699**, 479–483, DOI: 10.1016/j.jallcom.2016.12.401.

11 A. A. I. Khalil, A. S. H. M. Abd El-Gawad and A. S. Gadallah, Impact of Silver Dopants on Structural, Morphological, Optical, and Electrical Properties of Copper-Zinc Sulfide Thin Films Prepared via Sol-Gel Spin Coating Method, *Opt. Mater.*, 2020, **109**, 110250, DOI: 10.1016/j.optmat.2020.110250.

12 *Chalcogenide-Based Nanomaterials as Photocatalysts*, ed. M. M. Khan, Elsevier, 1st edn, 2021.

13 N. ul Ain, Z. U. Rehman, A. Aamir, Y. Khan, M. Rehman and D. Lin, Catalytic and Photocatalytic Efficacy of Hexagonal CuS Nanoplates Derived from Copper(II) Dithiocarbamate, *Mater. Chem. Phys.*, 2020, **242**, 122408, DOI: 10.1016/j.matchemphys.2019.122408.

14 M. Muneeb, B. Ismail, T. Fazal, R. A. Khan, A. M. Khan, M. Bilal, B. Muhammad and A. R. Khan, Water Treatment by Photodegradation on Orthorhombic Antimony Sulfide Powder and Effect of Key Operational Parameters Using Methyl Orange as a Model Pollutant, *Arabian J. Chem.*, 2018, **11**(7), 1117–1125, DOI: 10.1016/j.arabjc.2015.05.010.

15 B. Zhou, J. Song, C. Xie, C. Chen, Q. Qian and B. Han, Mo–Bi–Cd Ternary Metal Chalcogenides: Highly Efficient Photocatalyst for CO_2 Reduction to Formic Acid Under Visible Light, *ACS Sustainable Chem. Eng.*, 2018, **6**(5), 5754–5759, DOI: 10.1021/acssuschemeng.8b00956.

16 X. Fan, J. Zhang, Y. Yang, D. Xia, G. Dong, M. Li, L. Qiu, Y. Zhang and R. Fan, Synthesis of $AgBiSe_2$ via a Facile Low Temperature Aqueous Solution Route for Enhanced Photoelectric Properties Devices, *J. Solid State Chem.*, 2019, **277**, 686–692, DOI: 10.1016/j.jssc.2019.07.036.

17 M. Zhou, K. Xiao, X. Jiang, H. Huang, Z. Lin, J. Yao and Y. Wu, Visible-Light-Responsive Chalcogenide Photocatalyst Ba_2ZnSe_3: Crystal and Electronic Structure, Thermal, Optical, and Photocatalytic Activity, *Inorg. Chem.*, 2016, **55**(24), 12783–12790, DOI: 10.1021/acs.inorgchem.6b02072.

18 M. Zhou, X. Jiang, X. Jiang, K. Xiao, Y. Guo, H. Huang, Z. Lin, J. Yao, C.-H. Tung and L.-Z. Wu, *et al.*, $BaAu_2S_2$: A Au-Based Intrinsic Photocatalyst for High-Performance Visible-Light Photocatalysis, *Inorg. Chem.*, 2017, **56**(9), 5173–5181, DOI: 10.1021/acs.inorgchem.7b00319.

19 M. A. S. Andrade and L. H. Mascaro, Photoelectrocatalytic Reduction of Nitrobenzene on Bi-Doped $CuGaS_2$ Films, *Chemosphere*, 2018, **212**, 79–86, DOI: 10.1016/j.chemosphere.2018.08.071.

20 J. da Silveira Salla, K. da Boit Martinello, G. L. Dotto, E. García-Díaz, H. Javed, P. J. J. Alvarez and E. L. Foletto, Synthesis of Citrate–Modified $CuFeS_2$ Catalyst with Significant Effect on the Photo–Fenton Degradation Efficiency of Bisphenol a under Visible Light and near–Neutral PH, *Colloids Surf., A*, 2020, **595**, 124679, DOI: 10.1016/j.colsurfa.2020.124679.

21 Y. Han, Y. Yang, J. Zhao, X. Yin and W. Que, Facile One-Pot Synthesis of Ternary Copper-Tin-Chalcogenide Quantum Dots on Reduced Graphene Oxide for Enhanced Photocatalytic Activity, *Catal. Lett.*, 2018, **148**(10), 3112–3118, DOI: 10.1007/s10562-018-2525-y.

22 W. Wang, T. Ding, G. Chen, L. Zhang, Y. Yu and Q. Yang, Synthesis of Cu_2SnSe_3–Au Heteronanostructures with Optoelectronic and Photocatalytic Properties, *Nanoscale*, 2015, **7**(37), 15106–15110, DOI: 10.1039/C5NR04468E.

23 Q. Jia, Y. C. Zhang, J. Li, Y. Chen and B. Xu, Hydrothermal Synthesis of Cu_2WS_4 as a Visible-Light-Activated Photocatalyst in the Reduction of Aqueous Cr(VI), *Mater. Lett.*, 2014, **117**, 24–27, DOI: 10.1016/j.matlet.2013.11.110.

24 J. da Silveira Salla, G. L. Dotto, D. Hotza, R. Landers, K. da Boit Martinello and E. L. Foletto, Enhanced Catalytic Performance of $CuFeS_2$ Chalcogenide Prepared by Microwave-Assisted Route for Photo-Fenton Oxidation of Emerging Pollutant in Water, *J. Environ. Chem. Eng.*, 2020, **8**(5), 104077, DOI: 10.1016/j.jece.2020.104077.

25 B. Gao, L. Liu, J. Liu and F. Yang, Photocatalytic Degradation of 2,4,6-Tribromophenol over Fe-Doped $ZnIn_2S_4$: Stable Activity and Enhanced Debromination, *Appl. Catal., B*, 2013, **129**, 89–97, DOI: 10.1016/j.apcatb.2012.09.007.

26 D. Jing, M. Liu, Q. Chen and L. Guo, Efficient Photocatalytic Hydrogen Production under Visible Light over a Novel W-Based Ternary Chalcogenide Photocatalyst Prepared by a Hydrothermal Process, *Int. J. Hydrogen Energy*, 2010, **35**(16), 8521–8527, DOI: 10.1016/j.ijhydene.2010.04.170.

27 C. Nefzi, M. Souli, Y. Cuminal and N. Kamoun-Turki, Effect of Substrate Temperature on Physical Properties of Cu_2FeSnS_4 Thin Films for Photocatalysis Applications, *Mater. Sci. Eng., B*, 2020, 254, DOI: 10.1016/j.mseb.2020.114509.

28 Z. Han, N. Li, A. Shi, H. Wang, F. Ma, Y. Lv and R. Wu, One-Pot Synthesis of $Cu_2ZnSnSe_4$ Nanoplates and Their Visible-Light-Driven Photocatalytic Activity, *Nanoscale Res. Lett.*, 2018, **13**(1), 7, DOI: 10.1186/s11671-017-2428-7.

29 Y. Shi, Y. Chen, G. Tian, L. Wang, Y. Xiao and H. Fu, Hierarchical Ag/Ag < sub > 2 < sub > S/CuS Ternary Heterostructure Composite as an Efficient Visible-Light Photocatalyst, *ChemCatChem*, 2015, **7**(11), 1684–1690, DOI: 10.1002/cctc.201500121.

30 Y. Li, Y. Liu, G. Gao, Y. Zhu, D. Wang, M. Ding, T. Yao, M. Liu and W. You, L-Cysteine and Urea Synergistically-Mediated One-Pot One-Step Self-Transformed Hydrothermal Synthesis of p-Ag_2S/n-$AgInS_2$ Core-Shell Heteronanoflowers for Photocatalytic MO Degradation, *Appl. Surf. Sci.*, 2021, **548**, 149279, DOI: 10.1016/j.apsusc.2021.149279.

31 Y. Wang, Q. Zhang, Y. Li and H. Wang, Preparation of $AgInS_2$ Quantum Dot/In_2S_3 Co-Sensitized Photoelectrodes by a Facile Aqueous-Phase Synthesis Route and Their Photovoltaic Performance, *Nanoscale*, 2015, **7**(14), 6185–6192, DOI: 10.1039/C4NR06458E.

32 F. Deng, F. Zhong, D. Lin, L. Zhao, Y. Liu, J. Huang, X. Luo, S. Luo and D. D. Dionysiou, One-Step Hydrothermal Fabrication of Visible-Light-Responsive $AgInS_2$/$SnIn_4S_8$ Heterojunction for Highly-Efficient Photocatalytic Treatment of Organic Pollutants and Real Pharmaceutical Industry Wastewater, *Appl. Catal., B*, 2017, **219**, 163–172, DOI: 10.1016/j.apcatb.2017.07.051.

33 B. Liu, X. Li, Q. Zhao, J. Ke, M. Tadé and S. Liu, Preparation of $AgInS_2$/TiO_2 Composites for Enhanced Photocatalytic Degradation of Gaseous o-Dichlorobenzene under Visible Light, *Appl. Catal., B*, 2016, **185**, 1–10, DOI: 10.1016/j.apcatb.2015.12.003.

34 P. Ganguly, S. Mathew, L. Clarizia, R. S. Kumar, A. Akande, S. J. Hinder, A. Breen and S. C. Pillai, Ternary Metal Chalcogenide Heterostructure ($AgInS_2$-TiO_2) Nanocomposites for Visible Light Photocatalytic Applications, *ACS Omega*, 2020, **5**(1), 406–421, DOI: 10.1021/acsomega.9b02907.

35 J. Li, Z. Xia, D. Ma, G. Liu, N. Song, D. Xiang, Y. Xin, G. Zhang and Q. Chen, Improving Photocatalytic Activity by Construction of Immobilized Z-Scheme CdS/Au/TiO_2 Nanobelt Photocatalyst for Eliminating Norfloxacin from Water, *J. Colloid Interface Sci.*, 2021, **586**, 243–256, DOI: 10.1016/j.jcis.2020.10.088.

36 X.-L. Yin, S.-R. Han and L.-L. Li, CdS@MoS_2 Core@shell Nanorod Heterostructures for Efficient Photocatalytic Pollution Degradation with Good Stability, *Optik*, 2020, **220**, 165252, DOI: 10.1016/j.ijleo.2020.165252.

37 I. A. Mkhalid and A. Shawky, Visible Light-Active CdSe/RGO Heterojunction Photocatalyst for Improved Oxidative Desulfurization of Thiophene, *Ceram. Int.*, 2020, **46**(13), 20769–20776, DOI: 10.1016/j.ceramint.2020.05.033.

38 J. Hua, M. Wang, Y. Jiao, H. Li and Y. Yang, Strongly Coupled CdX (X = S, Se and Te) Quantum Dots/TiO_2 Nanocomposites for Photocatalytic Degradation of Benzene under Visible Light Irradiation, *Optik*, 2018, **171**, 95–106, DOI: 10.1016/j.ijleo.2018.06.049.

39 A. Zia, S. Hamid, M. F. Ehsan, S. U. Allah, M. N. Ashiq and A. Shah, Congo Red Photomineralization over Co_3O_4/CoTe Common Cation Nanocomposites, *J. Mater. Sci.: Mater. Electron.*, 2018, **29**(23), 20271–20279, DOI: 10.1007/s10854-018-0160-4.

40 Z. Otgonbayar, K. Youn Cho and W. C. Oh, Enhanced Photocatalytic Activity of CO_2 Reduction to Methanol through the Use of a Novel-Structured $CuCaAg_2Se$-Graphene-TiO_2 Ternary Nanocomposite, *New J. Chem.*, 2020, **44**(39), 16795–16809, DOI: 10.1039/d0nj03150j.

41 S. Vadivel, B. Paul, A. Habibi-Yangjeh, D. Maruthamani, M. Kumaravel and T. Maiyalagan, One-Pot Hydrothermal Synthesis of $CuCo_2S_4$/RGO Nanocomposites for Visible-Light Photocatalytic Applications, *J. Phys. Chem. Solids*, 2018, **123**, 242–253, DOI: 10.1016/j.jpcs.2018.08.011.

42 W. Y. Lim, M. Hong and G. W. Ho, In Situ Photo-Assisted Deposition and Photocatalysis of $ZnIn_2S_4$/Transition Metal Chalcogenides for Enhanced Degradation and Hydrogen Evolution under Visible Light, *Dalton Trans.*, 2016, **45**(2), 552–560, DOI: 10.1039/c5dt03775a.

43 N. R. Vempuluru, C. Kanakkampalayam Krishnan, R. Parnapalli, J. Velusamy, S. Marappan, S. Pitchaimuthu, M. Murikinati and S. Muthukonda Venkatakrishnan, Solar Hydrogen Generation from Organic Substance Using Earth Abundant CuS–NiO Heterojunction Semiconductor Photocatalyst, *Ceram. Int.*, 2021, **47**(7), 10206–10215, DOI: 10.1016/j.ceramint.2020.12.062.

44 M. Alhaddad and A. Shawky, CuS Assembled RGO Heterojunctions for Superior Photooxidation of Atrazine under Visible Light, *J. Mol. Liq.*, 2020, **318**, 114377, DOI: 10.1016/j.molliq.2020.114377.

45 Y.-J. Yuan, D. Chen, J. Zhong, L.-X. Yang, J. Wang, M.-J. Liu, W.-G. Tu, Z.-T. Yu and Z.-G. Zou, Interface Engineering of a Noble-Metal-Free 2D–2D MoS_2/Cu-$ZnIn_2S_4$ Photocatalyst for Enhanced Photocatalytic H_2 Production, *J. Mater. Chem. A*, 2017, **5**(30), 15771–15779, DOI: 10.1039/C7TA04410K.

46 Y. C. Zhang, L. Yao, G. Zhang, D. D. Dionysiou, J. Li and X. Du, One-Step Hydrothermal Synthesis of High-Performance Visible-Light-Driven SnS_2/SnO_2 Nanoheterojunction Photocatalyst for the Reduction of Aqueous Cr(VI), *Appl. Catal., B*, 2014, **144**, 730–738, DOI: 10.1016/j.apcatb.2013.08.006.

47 V. N. Rao, S. Pitchaimuthu, P. Ravi, M. Sathish, H. Han and S. M. Venkatakrishnan, Retorting Photocorrosion and Enhanced Charge Carrier Separation at CdSe Nanocapsules by Chemically Synthesized TiO_2 Shell for Photocatalytic Hydrogen Fuel Generation, *ChemCatChem*, 2020, **12**(11), 3139–3152, DOI: 10.1002/cctc.202000184.

48 J. C. Amaral-Júnior, A. A. P. Mansur, I. C. Carvalho and H. S. Mansur, Tunable Luminescence of Cu-In-S/ZnS Quantum Dots-Polysaccharide Nanohybrids by Environmentally Friendly Synthesis for Potential Solar Energy Photoconversion Applications, *Appl. Surf. Sci.*, 2021, **542**, 148701, DOI: 10.1016/j.apsusc.2020.148701.

49 A. Khan, M. Danish, U. Alam, S. Zafar and M. Muneer, Facile Synthesis of a Z-Scheme $ZnIn_2S_4$/MoO_3 Heterojunction with

Enhanced Photocatalytic Activity under Visible Light Irradiation, *ACS Omega*, 2020, **5**(14), 8188–8199, DOI: 10.1021/acsomega.0c00446.

50 D. Li, W. Wu, Y. Zhao and R. Qiao, Type-II Heterojunction Constructed by Ag_2S-Coupled ZnO Microspheres with Visible Light-Responsive Antibacterial Activity, *Mater. Lett.*, 2020, **271**, 127709, DOI: 10.1016/j.matlet.2020.127709.

51 M. S. Khan, A. Talib, S. Pandey, M. L. Bhaisare, G. Gedda and H.-F. Wu, Folic Acid Navigated Silver Selenide Nanoparticles for Photo-Thermal Ablation of Cancer Cells, *Colloids Surf., B*, 2017, **159**, 564–570, DOI: 10.1016/j.colsurfb.2017.07.070.

52 H. Qiu, S. Fang, G. Huang and J. Bi, A Novel Application of In_2S_3 for Visible Light-Driven Photocatalytic Inactivation of Bacteria: Kinetics, Stability, Toxicity and Mechanism, *Environ. Res.*, 2020, **190**(August), 110018, DOI: 10.1016/j.envres.2020.110018.

53 M. M. Khan, D. Pradhan and Y. Sohn, in *Nanocomposites for Visible Light-Induced Photocatalysis*, ed. M. M. Khan, D. Pradhan, Y. Sohn, Springer Series on Polymer and Composite Materials, Springer International Publishing, Cham, 2017, DOI: 10.1007/978-3-319-62446-4.

54 G. Yanalak, A. Sarılmaz, G. Karanfil, E. Aslan, F. Ozel and I. Hatay Patir, Enhanced Photocatalytic Hydrogen Evolution from Band-Gap Tunable Ag_2S:X (X = Ni, Co, Zn, Mn) Nanocrystals: Effect of Transition Metal Ions, *J. Photochem. Photobiol., A*, 2020, **394**, 112462, DOI: 10.1016/j.jphotochem.2020.112462.

55 Q. Li, H. Meng, P. Zhou, Y. Zheng, J. Wang, J. Yu and J. Gong, $Zn_{1-x}Cd_xS$ Solid Solutions with Controlled Bandgap and Enhanced Visible-Light Photocatalytic H_2-Production Activity, *ACS Catal.*, 2013, **3**(5), 882–889, DOI: 10.1021/cs4000975.

56 S. Chen, X. G. Gong, A. Walsh and S. H. Wei, Crystal and Electronic Band Structure of Cu_2ZnSnX_4 (X = S and Se) Photovoltaic Absorbers: First-Principles Insights, *Appl. Phys. Lett.*, 2009, **94**(4), 041903, DOI: 10.1063/1.3074499.

57 Z. Lv, W. Li, X. Cheng, B. Liu, Z. Guo, T. Zhuang and C. Zhang, Constructing Internal Electric Field in CdS via Bi, Ni Co-Doping Strategy for Enhanced Visible-Light H_2 Production, *Appl. Surf. Sci.*, 2021, **556**, 149758, DOI: 10.1016/j.apsusc.2021.149758.

58 E. Garskaite, G.-T. Pan, T. C. K. Yang, S.-T. Huang and A. Kareiva, The Study of Preparation and Photoelectrical Properties of Chemical Bath Deposited Zn, Sb and Ni-Doped $CuInS_2$ Films for Hydrogen Production, *Sol. Energy*, 2012, **86**(9), 2584–2591, DOI: 10.1016/j.solener.2012.05.031.

59 Y.-Y. Chai, D.-P. Qu, D.-K. Ma, W. Chen and S. Huang, Carbon Quantum Dots/Zn^{2+} Ions Doped-CdS Nanowires with Enhanced Photocatalytic Activity for Reduction of 4-Nitroaniline to p-Phenylenediamine, *Appl. Surf. Sci.*, 2018, **450**, 1–8, DOI: 10.1016/j.apsusc.2018.04.121.

60 C. Guo, L. Li, F. Chen, J. Ning, Y. Zhong and Y. Hu, One-Step Phosphorization Preparation of Gradient-P-Doped CdS/CoP Hybrid Nanorods Having Multiple Channel Charge Separation for Photocatalytic Reduction of Water, *J. Colloid Interface Sci.*, 2021, **596**, 431–441, DOI: 10.1016/j.jcis.2021.03.170.

61 Y. Zhu, E. Li, H. Zhao, S. Shen, J. Wang, Z. Lv, M. Liu, Y. Wen, L. Lu and J. Liu, Carbon Nitride Derived Carbon and Nitrogen Co-Doped CdS for Stable Photocatalytic Hydrogen Evolution, *Surf. Interfaces*, 2021, **25**, 101262, DOI: 10.1016/j.surfin.2021.101262.

62 A. P. Gaikwad, C. A. Betty, J. Jagannath, A. Kumar and R. Sasikala, Microflowers of Pd Doped ZnS for Visible Light Photocatalytic and Photoelectrochemical Applications, *Mater. Sci. Semicond. Process.*, 2018, **86**, 139–145, DOI: 10.1016/j.mssp.2018.05.020.

63 R. Ranjith, V. Krishnakumar, S. Boobas, J. Venkatesan and J. Jayaprakash, An Efficient Photocatalytic and Antibacterial Performance of Ni/Ce-Codoped CdS Nanostructure under Visible Light Irradiation, *ChemistrySelect*, 2018, **3**(32), 9259–9267, DOI: 10.1002/slct.201801485.

64 X. Yang, Z. Wang, X. Lv, Y. Wang and H. Jia, Enhanced Photocatalytic Activity of Zn-Doped Dendritic-like CdS Structures Synthesized by Hydrothermal Synthesis, *J. Photochem. Photobiol., A*, 2016, **329**, 175–181, DOI: 10.1016/j.jphotochem.2016.07.005.

65 D. Aldakov, A. Lefrançois and P. Reiss, Ternary and Quaternary Metal Chalcogenide Nanocrystals: Synthesis, Properties and Applications, *J. Mater. Chem. C*, 2013, **1**(24), 3756, DOI: 10.1039/c3tc30273c.

66 D. Zhao, T. Wu and Y. Zhou, Dual II Heterojunctions Metallic Phase MoS_2/ZnS/ZnO Ternary Composite with Superior Photocatalytic Performance for Removing Contaminants, *Chem. – Eur. J.*, 2019, **25**(41), 9710–9720, DOI: 10.1002/chem.201901715.

67 L. Mao, H. Liu, S. Liu, Q. Ba, H. Wang, L. Gao, X. Li, C. Huang and W. Chen, Pt-Ru Bi-Metal Co-Catalyst: Preparation, Characterization and Its Effect on CdS's Activity for Water Splitting under Visible Light, *Mater. Res. Bull.*, 2017, **93**, 9–15, DOI: 10.1016/j.materresbull.2017.03.035.

68 Z. Zheng, T. Wang, F. Han, Q. Yang and B. Li, Synthesis of Ni Modified Au@CdS Core–Shell Nanostructures for Enhancing Photocatalytic Coproduction of Hydrogen and Benzaldehyde under Visible Light, *J. Colloid Interface Sci.*, 2022, **606**, 47–56, DOI: 10.1016/j.jcis.2021.07.150.

69 P. Salarizadeh, M. B. Askari, N. Askari and N. Salarizadeh, Ternary Transition Metal Chalcogenides Decorated on RGO as an Efficient Nanocatalyst towards Urea Electro-Oxidation Reaction for Biofuel Cell Application, *Mater. Chem. Phys.*, 2020, **239**(2019), 121958, DOI: 10.1016/j.matchemphys.2019.121958.

70 A. Balapure, H. Mude, P. Tata, J. Ray Dutta and R. Ganesan, Sublimable Xanthate-Mediated Solid-State Synthesis of Highly Interspersed g-C_3N_4/Ag_2S Nanocomposites Exhibiting Efficient Bactericidal Effects Both under Dark and Light Conditions, *J. Environ. Chem. Eng.*, 2021, **9**(5), 106065, DOI: 10.1016/j.jece.2021.106065.

71 W. Zuo, L. Liang, F. Ye and S. Zhao, Construction of Visible Light Driven Silver Sulfide/Graphitic Carbon Nitride p-n Heterojunction for Improving Photocatalytic Disinfection, *Chemosphere*, 2021, **283**, 131167, DOI: 10.1016/j.chemosphere.2021.131167.

72 R. Chen, P. Wang, J. Chen, C. Wang and Y. Ao, Synergetic Effect of MoS_2 and MXene on the Enhanced H_2 Evolution Performance of CdS under Visible Light Irradiation, *Appl. Surf. Sci.*, 2019, **473**, 11–19, DOI: 10.1016/j.apsusc.2018.12.071.

73 P. Liang, L. Yuan, K. Du, L. Wang, Z. Li, H. Deng, X. Wang, S.-Z. Luo and W. Shi, Photocatalytic Reduction of Uranium(VI) under Visible Light with 2D/1D Ti3C2/CdS, *Chem. Eng. J.*, 2021, **420**, 129831, DOI: 10.1016/j.cej.2021.129831.